Adiabatic quenches and characterization of amplitude excitations in a continuous quantum phase transition

Thai M. Hoang[a], Hebbe M. Bharath[a], Matthew J. Boguslawski[a], Martin Anquez[a], Bryce A. Robbins[a], and Michael S. Chapman[a,1]

[a]School of Physics, Georgia Institute of Technology, Atlanta, GA 30332-0430

Spontaneous symmetry breaking occurs in a physical system whenever the ground state does not share the symmetry of the underlying theory, e.g., the Hamiltonian. This mechanism gives rise to massless Nambu–Goldstone modes and massive Anderson–Higgs modes. These modes provide a fundamental understanding of matter in the Universe and appear as collective phase or amplitude excitations of an order parameter in a many-body system. The amplitude excitation plays a crucial role in determining the critical exponents governing universal nonequilibrium dynamics in the Kibble–Zurek mechanism (KZM). Here, we characterize the amplitude excitations in a spin-1 condensate and measure the energy gap for different phases of the quantum phase transition. At the quantum critical point of the transition, finite-size effects lead to a nonzero gap. Our measurements are consistent with this prediction, and furthermore, we demonstrate an adiabatic quench through the phase transition, which is forbidden at the mean field level. This work paves the way toward generating entanglement through an adiabatic phase transition.

adiabatic quenches | amplitude excitations | quantum phase transition

The amplitude mode and phase mode describe two distinct excitation degrees of freedom of a complex order parameter $\psi = Ae^{i\phi}$ appearing in many quantum systems such as the order parameter of the Ginzburg–Laudau superconducting phase transition (1) and the two-component quantum field of the Nambu–Goldstone–Anderson–Higgs matter field model (2–5). In a zero-dimensional system of an interacting spin-1 condensate, the transverse spin, $\mathbf{S}_\perp$, plays the role of an order parameter in the quantum phase transition (QPT) with $\mathbf{S}_\perp$ being zero in the polar (P) phase and nonzero in the broken axisymmetry (BA) phase (Fig. 1A). Representing the transverse spin vector as a complex number, $\mathbf{S}_\perp = S_x + iS_y$, with the real and imaginary parts being expectation values of spin-1 operators, the amplitude mode corresponds to the amplitude oscillation of $\mathbf{S}_\perp$.

The amplitude mode can be studied in different spinor phases by tuning the relative strengths of the quadratic Zeeman energy per particle $q \propto B^2$ and spin interaction energy c of the condensate (6) by varying the magnetic field strength B (Fig. 1). In the P phase, both the effective spinor potential energy V and the ground state (GS) spin vector have SO(2) rotational symmetry about the vertical axis (Fig. 1A), and there are two degenerate collective amplitude modes along the radial directions about the GS located at the bottom of the parabolic bowl. These amplitude excitations are gapped modes, which vary both the amplitude of $\mathbf{S}_\perp$ and the energy.

In the BA phase, the effective spinor potential energy V acquires a Mexican-hat shape with the GS occupying the minimal energy ring of radius $\sqrt{4c^2 - q^2}/(2|c|)$. The GS spin vector, $\mathbf{S}_\perp$ (orange arrow in Fig. 1A), spontaneously breaks the SO(2) symmetry and acquires a definite direction (7, 8). This broken symmetry induces a massless Nambu–Goldstone (NG) mode in which it costs no energy for the spin vector to rotate about the vertical axis. Recently, the magnetic dipolar interaction was used to open a gap in the NG mode by breaking the rotational symmetry of the spin interaction (9). In our condensate, the magnetic dipolar interaction can be ignored due to spatial isotropy, and therefore, the NG mode in the BA phase remains gapless. The other excitation, the amplitude mode, manifests itself as an amplitude oscillation of the transverse spin in the radial direction. This amplitude mode is similar to the massive mode in the Goldstone model (3).

In this work, we measure the amplitude modes in a spin-1 Bose–Einstein condensate (BEC) through measurements of very low amplitude excitations from the GS. The results show a quantitative agreement with gapped excitation theory (10–12) and provide a platform to probe the amplitude excitation, which plays a crucial role in the KZM in spinor condensates (11, 13–15). Although in the thermodynamic limit the amplitude mode energy gap goes to zero at the quantum critical point (QCP), a small size-dependent gap persists for finite-size systems (12). Measurements of the energy gap near the QCP are challenging; however, our results are consistent with a small nonzero gap. Furthermore, by using a very slow, optimized magnetic field ramp, we demonstrate an adiabatic quench across the QCP. Such adiabatic quenches in finite-sized systems underlie proposals for generating massively entangled spin states including Dicke states (12) and are fundamental to the ideas of adiabatic quantum computation (16).

The experiments use a tightly confined ^{87}Rb BEC with $N = 40,000$ atoms in optical traps such that spin domain formation is energetically suppressed. The Hamiltonian describing

Significance

Symmetry-breaking phase transitions play important roles in many areas of physics, including cosmology, particle physics, and condensed matter. The freezing of water provides a familiar example: The translational and rotational symmetries of water are reduced upon crystallization. In this work, we investigate symmetry-breaking phase transitions of the magnetic properties of an ultracold atomic gas in the quantum regime. We measure the excitations of the quantum magnets in different phases and show that the excitation energy (gap) remains finite at the phase transition. We exploit the nonzero gap to demonstrate an adiabatic (reversible) quench across the phase transition. Adiabatic quantum quenches underlie proposals for generating massively entangled spin states and are fundamental to the ideas of adiabatic quantum computation.

PHYSICS

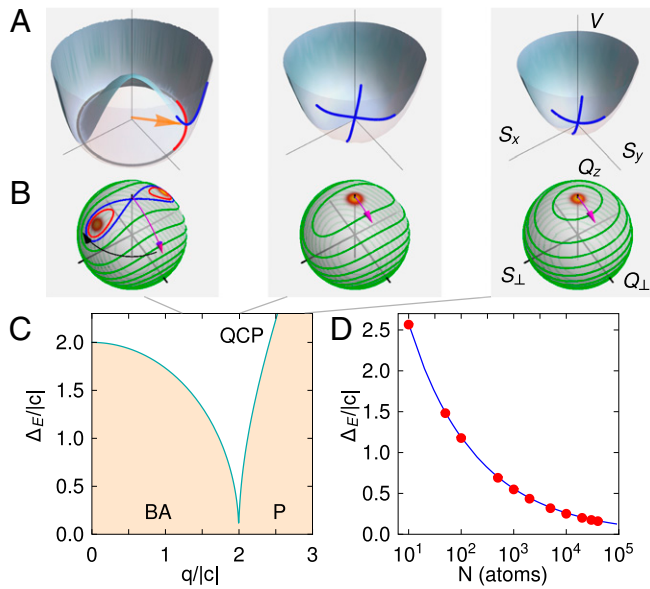**Fig. 1.** (*A*) Effective spinor potential energy V in the BA phase ($q/|c| < 2$), at the QCP ($q/|c| = 2$), and in the P phase ($q/|c| > 2$). In the P phase, there are two gapped modes (blue lines) along the radial direction about the GS. In the BA phase, the GS occupies a minimum energy ring (gray circle) with one gapped mode along the radial direction (blue line) and one NG mode (red line) in the azimuthal direction. (*B*) The GS on the $\{S_\perp, Q_\perp, Q_z\}$ unit spheres is represented by a red-shaded region. Coherent orbiting (phase winding) dynamics are represented by red (green) curves and the blue curve is the separatrix. The magenta (black) arrow represents the radio-frequency (microwave) pulse used for the initial state preparation (*Supporting Information*). (*C*) The energy gap for 40,000 atoms (cyan curve) is calculated from the eigenvalues of the quantum Hamiltonian (*Supporting Information*). (*D*) The energy gap at the QCP (blue solid line) calculated from the eigenvalues of the quantum Hamiltonian matches the GS oscillation frequencies from simulations (red circles).

this spin system in a bias magnetic field B along the z axis is (17–21)

$$\hat{H} = \tilde{c}\hat{S}^2 - q(\hat{Q}_z - N)/2, \qquad [1]$$

where $\hat{S}^2$ is the total collective spin-1 operator and $\hat{Q}_z$ is proportional to the spin-1 quadrupole moment, $\hat{Q}_{zz}$. The coefficient $\tilde{c}$ is the collisional spin interaction energy per particle integrated over the condensate and quadratic Zeeman energy per particle $q = q_z B^2$ with $q_z = 72$ Hz/G^2 (hereafter, $h = 1$). The longitudinal magnetization $\langle \hat{S}_z \rangle$ is a constant of the motion ($\langle \hat{S}_z \rangle = 0$ for these experiments); hence the first-order linear Zeeman energy $p\hat{S}_z$ with $p \propto B$ can be ignored. The spin-1 coherent states can be represented on the surface of a unit sphere shown in Fig. 1*B* with axes $\{S_\perp, Q_\perp, Q_z\}$, where the expectation value of transverse spin is $S_\perp^2 = S_x^2 + S_y^2$, $Q_\perp$ is the transverse off-diagonal nematic moment $Q_\perp^2 = Q_{xz}^2 + Q_{yz}^2$, and $Q_z = 2\rho_0 - 1$, where ρ_0 is the fractional population in the $|F = 1, m_F = 0\rangle$ state. In this representation, the coherent dynamics evolve along the constant energy contours of $\mathcal{H} = (1/2)cS_\perp^2 - (1/2)q(Q_z - 1)$, where $c = 2N\tilde{c}$ (22–24) (red and green orbits in Fig. 1*B*). The phase space for the single-mode spin-1 condensate is similar to that for the Lipkin–Meshkov–Glick (LMG) model (25), which in turn describes the infinite coordination number limit of the XY model or quantum Ising model (26). The dynamics of the QPT in these zero-dimensional quantum systems have been explored theoretically and experimental realizations include the double-well Bose–Hubbard (27, 28), pseudospin-1/2 BEC (29, 30), and many-atom cavity quantum electrodynamics systems (31).

In the mean-field (large atom number) limit, quantum fluctuations can be ignored and the wavefunction for each spin state, $m_F = 0, \pm 1$, can be represented as a complex vector with components, $\psi_{0,\pm1} = \sqrt{\rho_{0,\pm1}}\exp(i\theta_{0,\pm1})$. Using Bogoliubov analysis (10) and mean-field theory (24, 32), the energy gap of the amplitude mode in the P phase and the BA phase in the long-wavelength limit corresponds to the oscillation frequency of small excitations in ρ_0 from the GS

$$\Delta_P \equiv f_P = 2\sqrt{q(q + 2c)}, \quad \Delta_{BA} \equiv f_{BA} = 2\sqrt{c^2 - q^2/4}. \qquad [2]$$

Here the energy gap is Δ_E ($\equiv \Delta_P$ and Δ_{BA}) and coherent oscillation frequency is f ($\equiv f_P$ and f_{BA}). Although these relations show a vanishing gap at the QCP, quantum fluctuations due to finite atom number result in a nonzero gap. In the quantum theory, the energy gap can be exactly calculated from the eigenenergy values of the Hamiltonian in Eq. **1** (*Supporting Information*). Fig. 1*C* shows the energy gap between the GS and the first excited state with a small nonzero gap at the QCP as a result of a finite atom number. Fig. 1*D* shows the relation of energy gap at the QCP to the atom number in condensates ranging from 10^1 to 10^5 atoms, which scales as $\Delta_E \propto N^{-1/3}$ (12). The energy gap curve compares well to the oscillation frequencies of GS spinor population ρ_0 obtained from quantum simulations (*Supporting Information*) for a broad range of atom numbers (red circles in Fig. 1*D*). The equivalence relation between the energy gap and the coherent oscillation (32) frequency in Eq. **2** is a general statement connecting the amplitude modes to the observable dynamics and is key to this study.

Energy Gap Measurement

To characterize the energy gap Δ_E, we measure coherent dynamics for states initialized close to the GS (Fig. 1*B*) for different values of $q/|c|$ ranging from 0.1 to 3 and fit the measurements to sinusoidal functions to determine the oscillation frequencies (*Supporting Information*). For each $q/|c|$ value, several measurements of the population ρ_0 are made for a series of initial states approaching the GS as illustrated in Fig. 2*A*. The GS population $\rho_{0,GS}$ can be obtained by minimizing the spinor energy (*Supporting Information*) (24)

$$\rho_{0,GS} = 1 \ (P), \quad \rho_{0,GS} = 1/2 + q/(4|c|)(BA). \qquad [3]$$

The oscillation amplitude of ρ_0 has a lower limit given by the Heisenberg standard quantum limit (SQL $= N^{-1/2}$) projected onto the ρ_0 axis ($\propto Q_z$ axis in Fig. 1*B*) (21); hence the best estimate of the energy gap is obtained from the measurement with the lowest observable oscillation amplitude. An alternate method to determine the energy gap for states centered on the pole is to measure the oscillations of the transverse spin fluctuations, $\Delta S_\perp$. Although this method requires many more data because the signal is in the fluctuations instead of the mean value, it provides higher contrast for states localized at the pole. Measurements obtained with this technique at the QCP are shown in Fig. 2*B* for a state prepared in the polar GS (*Supporting Information*).

The results of the energy gap measurements are shown in Fig. 2*C* for both methods. Overall, the measurements capture the characteristics of energy gap predicted by gapped excitation theory for a spin-1 BEC (10–12). In the P phase, the energy gap data show a good agreement with the theoretical prediction within the uncertainty of the measurements. In the BA phase, the measured gap data are also in reasonable agreement with the theory; however, the measured values are 20% lower than the theory for the smallest values of $q/|c| < 1$. This finding is possibly a result of small violations of the single-mode approximation or the presence of a small thermal fraction, both of which would be more significant in this spin interaction-dominated regime. In a
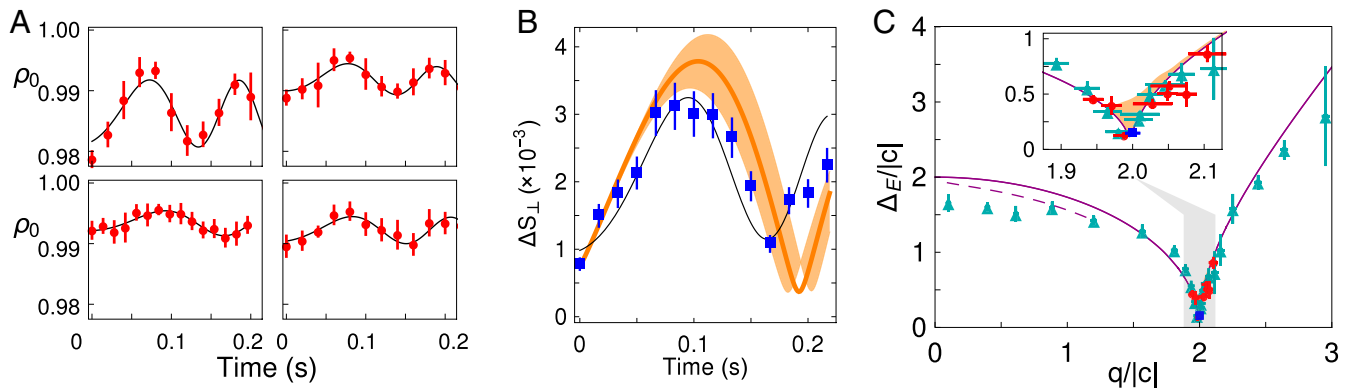
Fig. 2. Energy gap measurements. (*A*) Coherent oscillation data (red circles) obtained at $q/|c| = 2.03$. In clockwise order, the oscillation amplitude decreases as the initial state is prepared closer to the GS. Each data point is an average of 10 measurements and the data are fitted to a sinusoidal function with a varying frequency (solid line). (*B*) The time evolution of $\Delta S_\perp$ data (blue squares) at the QCP ($q/|c| = 2$) is fitted to a sinusoidal function (solid line). Each data point is the noise of 45 measurements. The corresponding simulation is represented by an orange curve with the shaded region being $q/|c| = 2 \pm 0.005$. (*C*) The energy gap Δ_E for different $q/|c|$ values is obtained from the frequency fits of coherent oscillation data. Circles (triangles) are obtained from an average of 10 (or 3) measurements of ρ_0 coherent oscillation, and the blue square is the frequency fit of $\Delta S_\perp$ dynamics. The theoretical energy gap is represented by the purple curve. *Inset* shows the region around the QCP with the shaded orange region being the energy gap for an imperfect initialization of the GS (main text). The dashed line shows the theoretical energy gap when the initial population ρ_0 is about 0.05 away from the actual GS, reflecting an oscillation amplitude of 0.05.

study of an antiferromagnetic condensate, using an initial state ($\rho_0 = 0.5$) prepared far away from the antiferromagnetic GS ($\rho_{0,AGS} = 1$), slightly lower oscillation frequencies than those in the theory were also observed (33); it was suggested that these resulted from excess magnetization noise from the radio frequency (RF) pulse of the initial state preparation; however, this noise is not large enough to explain the difference in our measurements.

In the neighborhood of the QCP, the energy gap decreases dramatically. As shown in Fig. 2*C*, *Inset*, the measurements are in good agreement with the theoretical prediction in this region. For measurements at $q = 2|c|$, the minimum measured gap is $\Delta_E = 0.15(1)|c|$, which is consistent with the nonzero gap predicted by the quantum theory, $\Delta_{E,th} = 0.165|c|$; here $c \approx -7.5(1)$ Hz (*Supporting Information*). We point out, however, that there are experimental challenges to these measurements. The initial state is prepared in the high magnetic field GS ($q/|c| = 38$). This state has symmetric $\sqrt{N}$ fluctuations in the $S_\perp, Q_\perp$ plane. When the condensate is rapidly quenched to a lower $q/|c|$ for the energy gap measurement, this projects the condensate to slightly excited states of the final $q/|c|$ Hamiltonian. The subsequent evolution of this state will have an oscillation frequency higher than the calculated gap frequency, particularly in the region $1.95 \leq q/|c| \leq 2.05$. We can accurately calculate this effect, and the results are indicated by the orange-shaded region in Fig. 2*C*.

A further complication in the measurement at the QCP is that the value $q/|c|$ is not truly constant during the measurement of the gap, but drifts to slightly higher values because of a reduction of density due to the finite lifetime of the condensate. The spin interaction energy depends on the density and atom number as $c(t) \propto n(t) \propto N(t)^{2/5}$. For these measurements, the condensate lifetime was 1.6(1) s, which results in a drift of $\Delta q/|c| = 0.05$ in 100 ms in the neighborhood of the QCP. The atom loss is taken into account in the simulations, an example of which is shown in Fig. 2*C*, and the energy gap is determined by the frequency at $t = 0$. Despite these challenges to the measurements near the QCP, the data indicate the presence of a nonzero gap that is of the same size as predicted by theory.

In the BA phase of a $\langle \hat{S}_z \rangle = 0$ spin-1 BEC, two of the three excitation modes (*Supporting Information*) are massless NG modes that appear due to broken global symmetries. The third mode is a massive amplitude mode with a dispersion relation: $E^2(k_0) = \Delta_E^2 + (2c\hbar/m)^2 k_0^2$ with k_0 being the wavenumber and m being the atomic mass (10, 11). The energy gap Δ_E is equivalent

to the rest mass energy of the quasiparticle corresponding to the excitation mode. Our experiments are in the long-wavelength limit in which the wave vector approaches zero, $\mathbf{k}_0 \to 0$. The massive amplitude mode that appears when a global symmetry is broken has properties analogous to those of the Higgs mode, which relates to the amplitude fluctuation of the order parameter of the phase transition. Such a Higgs-like mode has been observed as a collective excitation in the superfluid/Mott insulator transition as an amplitude fluctuation of a complex order parameter (34), in the XY model of antiferromagnetic materials as an amplitude fluctuation of the spin vector (35), in superconducting systems (36–39), and here as the amplitude mode of the spin-1 BEC in the BA phase.

Adiabatic QPT

In the thermodynamic ($N \to \infty$) limit, the vanishing gap at the QPT prohibits adiabatic crossing between phases and gives rise to excitations characterized by the Kibble–Zurek mechanism (KZM). However, the opening of the gap at the QCP due to finite-size effects makes it possible, in principle, to cross the QCP adiabatically using a carefully tailored ramp from $q \gg 2|c|$ to $q < 2|c|$, while remaining in the GS of the Hamiltonian. Recently, adiabaticity in sodium spin-1 condensates has been studied (40); however, these experiments were performed using condensates with nonzero longitudinal magnetization ($\langle \hat{S}_z \rangle \neq 0$) that do not have a QCP. Here, we focus on the very challenging case of the small energy gap at the QCP.

Due to the small size of the gap, the ramp in q needs to be very slow in the region of $2|c|$ to maintain adiabaticity. To allow longer ramps, we used a single-focus dipole trap in which the condensate lifetime is 15–19 s. To determine the optimal ramp, we performed simulations using measured values of the trap lifetime, the atom number, and the spin interaction energy. The ramp is determined from a piecewise optimization of the Landau–Zener adiabaticity parameter $(d\Delta_E/dt)(1/\Delta_E^2)$ (41–44) and includes the effects of atom loss on c (*Supporting Information*). The simulations (45, 46) show that it is possible to adiabatically cross the phase transition in $\sim$35 s, starting with a condensate initially containing 40,000 atoms; here we use an adiabatic invariant to determine the condition for adiabaticity (44, 47).

The experiment starts with atoms at the GS in the polar phase at a high magnetic field, $q/|c| = 140$. Then, the magnetic field is ramped through the QCP to $q/|c| = 1.33$ in 35 s along the trajectory
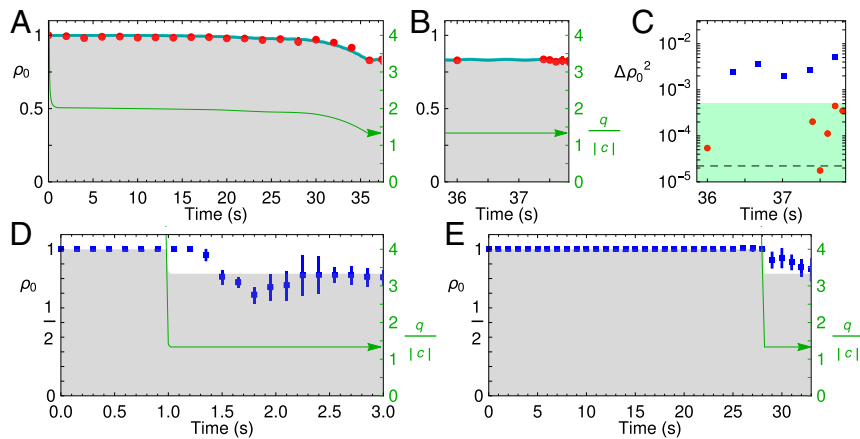
Fig. 3. Adiabatic and nonadiabatic dynamics. (*A*–*C*) Adiabatic dynamics of population ρ_0 and the uncertainty $\Delta\rho_0$ (main text). (*D* and *E*) Nonadiabatic dynamics of population ρ_0 of 1-s and 28-s linear ramp from $q/|c| = 140 \rightarrow 1.33$. Red circles (blue squares) are the adiabatic (nonadiabatic) measurements, gray-shaded regions are the theoretical $\rho_{0,\text{GS}}$ values, green arrow lines represent the ramp of $q/|c|$ (vertical axis on the right), and cyan curves represent the dynamics simulation of ρ_0 with the corresponding $q/|c|$ ramp. Each adiabatic data point is an average of 3 measurements and each nonadiabatic data point is an average of 15 measurements.

represented by the green line in Fig. 3*A*. The measured evolution of the population ρ_0 is shown in the same graph and compared with that predicted by the simulation. The data show excellent agreement with the theoretical values for the evolving GS population $\rho_{0,\text{GS}}$ (Eq. **3**), which provides a strong indication of adiabaticity.

There are about 9,000 atoms remaining after the adiabatic ramp. The theoretical value of the GS population and uncertainty is $\rho_{0,\text{GS}} = 0.833 \pm 0.0047$, where the uncertainty is the SQL for 9,000 atoms, projected onto the ρ_0 axis ($\propto Q_z$ axis in Fig. 1*B*) (*Supporting Information*). Immediately after the adiabatic ramp ($t \approx 36$ s), the measured mean population and fluctuations are $\rho_0 = 0.830 \pm 0.007$, which are very close to the theoretical values and further indicate adiabiticity. Following the adiabatic ramp, the ratio $q/|c| = 1.33$ is held constant for 2 s to verify that the system remains in the GS. As shown in Fig. 3*B*, the mean value of ρ_0 stays close to the theoretical value $\rho_{0,\text{GS}}$. In Fig. 3*C*, the variance $\Delta\rho_0^2$ is plotted. Although the measurements of $\Delta\rho_0^2$ (red circles) tend above the theoretical SQL squared (dashed line) after holding, atom loss increases fluctuations in the spin populations (assuming uncorrelated losses) to the level shown in the green-shaded region (*Supporting Information*).

For comparison, in Fig. 3 *D* and *E* we show data from non-adiabatic ramps from $q/|c| = 140 \rightarrow 1.33$. In Fig. 3*D*, a 1-s linear ramp is used, whereas in Fig. 3*E*, a 28-s ramp is used. In both cases, the spin population ρ_0 does not follow the theoretical GS population during the ramp and the variance $\Delta\rho_0^2$ grows dramatically. The fluctuations at the end of the 28-s ramp are compared with those from the adiabatic ramp in Fig. 3*C* (blue squares), and it is clear that the nonadiabaticity gives rise to increased fluctuations.

Adiabatically crossing the QPT in a spin-1 zero magnetization condensate is predicted to generate massively entangled spin states (12). Broadly speaking, this is an example of the fundamental principle underlying adiabatic quantum computing, in which the initial, simple GS is transformed into a highly entangled final GS by tuning the Hamiltonian adiabatically through a QCP. This final GS of the Hamiltonian is a solution to a computation problem (16). In our case, the final state for a ramp to $q = 0$ is predicted to be the Dicke state $|S = N, S_z = 0\rangle$. In this study, we stop the adiabatic ramp at $q/|c| = 1.33$. The

entanglement of the GS at this $q/|c|$ can be calculated as in ref. 12, $\xi = (\langle\hat{S}_x^2\rangle + \langle\hat{S}_y^2\rangle)N/(1 + 4\langle(\Delta\hat{S}_z)^2\rangle N^2)$. The uncertainty in transverse magnetization is $\langle\hat{S}_x^2\rangle + \langle\hat{S}_y^2\rangle \approx 1 - (2\rho_0 - 1)^2$. In the ideal case, the longitudinal magnetization is zero and conserved $\langle(\Delta\hat{S}_z)^2\rangle \rightarrow 0$, and the expected entanglement is $\xi = 0.56N$ or roughly 5,000 atoms are entangled out of 9,000 atoms at the end of the adiabatic ramp. However, atom loss induces noise in the magnetization, $\Delta S_z \approx 0.5\%$, in our experiment. This small magnetization noise reduces the entanglement to $\xi < 1$ atom.

In summary, we have explored the amplitude mode in small spin-1 condensates. The energy gap measurements show evidence of a nonzero gap at the QCP arising from finite-size effects, and using a carefully tailored slow ramp of the Hamiltonian parameters, we have adiabatically crossed the QCP with no apparent excitation of the system. We hope that this work stimulates similar investigations in related many-body systems, and in particular, we anticipate that the results of this study could directly inform investigations in double-well Bose–Josephson junction systems, (pseudo)spin-1/2 interacting systems (48, 49), and the Lipkin–Meshkov–Glick (LMG) model (43, 50), which share similar Hamiltonians.

Materials and Methods

The experiment is carried out using small condensates of 40,000 atoms in the $F = 1$ hyperfine GS of ^{87}Rb. In the energy gap experiment, atoms are confined in a spherical optical dipole force trap with trap frequencies $\sim 2\pi \times 160$ Hz, formed by crossing the focus of a 10.6-μm wavelength laser with an 850-nm wavelength laser. This tight confinement ensures that the condensate is well described by the single-mode approximation (SMA), such that the spin dynamics can be considered separately from the spatial dynamics (17–19). The spin interaction energy $c \approx -7.5(1)$ Hz and trap lifetime is $\approx 1.6(1)$ s. The spin populations of the condensate are measured by releasing the trap and allowing them to expand in a Stern–Gerlach magnetic field gradient to separate the m_F spin components. The atoms are probed for 200 μs with three pairs of counter-propagating orthogonal laser beams, and the fluorescence signal collected by a CCD camera is used to determine the number of atoms in each spin component.

1. Landau LD, Ginzburg VL (1950) On the theory of superconductivity. *Zh Eksp Teor Fiz* 20:1064–1082.
2. Nambu Y (1960) Quasi-particles and gauge invariance in the theory of superconductivity. *Phys Rev* 117(3):648.
3. Goldstone J (1961) Field theories with superconductor solutions. *Nuovo Cim* 19(1):154–164.
4. Anderson PW (1963) Plasmons, gauge invariance, and mass. *Phys Rev* 130:439–442.
5. Higgs PW (1964) Broken symmetries and the masses of gauge bosons. *Phys Rev Lett* 13:508–509.
6. Stenger J, et al. (1998) Spin domains in ground-state Bose-Einstein condensates. *Nature* 396(6709):345–348.

7. Sadler LE, Higbie JM, Leslie SR, Vengalattore M, Stamper-Kurn DM (2006) Spontaneous symmetry breaking in a quenched ferromagnetic spinor Bose-Einstein condensate. *Nature* 443(7109):312–315.

8. Sachdev S (2011) *Quantum Phase Transitions* (Cambridge Univ Press, Cambridge, UK).

9. Marti GE, et al. (2014) Coherent magnon optics in a ferromagnetic spinor Bose-Einstein condensate. *Phys Rev Lett* 113(15):155302.

10. Murata K, Saito H, Ueda M (2007) Broken-axisymmetry phase of a spin-1 ferromagnetic Bose-Einstein condensate. *Phys Rev A* 75:013607.

11. Lamacraft A (2007) Quantum quenches in a spinor condensate. *Phys Rev Lett* 98(16):160404.

12. Zhang Z, Duan LM (2013) Generation of massive entanglement through an adiabatic quantum phase transition in a spinor condensate. *Phys Rev Lett* 111(18):180401.

13. Saito H, Kawaguchi Y, Ueda M (2007) Kibble-Zurek mechanism in a quenched ferromagnetic Bose-Einstein condensate. *Phys Rev A* 76(4):043613.

14. Damski B, Zurek WH (2007) Dynamics of a quantum phase transition in a ferromagnetic Bose-Einstein condensate. *Phys Rev Lett* 99(13):130402.

15. Anquez M, et al. (2016) Quantum Kibble-Zurek mechanism in a spin-1 Bose-Einstein condensate. *Phys Rev Lett* 116(15):155301.

16. Farhi E, et al. (2001) A quantum adiabatic evolution algorithm applied to random instances of an NP-complete problem. *Science* 292(5516):472–475.

17. Ho TL (1998) Spinor Bose condensates in optical traps. *Phys Rev Lett* 81:742–745.

18. Ohmi T, Machida K (1998) Bose-Einstein condensation with internal degrees of freedom in alkali atom gases. *J Phys Soc Jpn* 67(6):1822–1825.

19. Law CK, Pu H, Bigelow NP (1998) Quantum spins mixing in spinor Bose-Einstein condensates. *Phys Rev Lett* 81:5257–5261.

20. Mias GI, Cooper NR, Girvin SM (2008) Quantum noise, scaling, and domain formation in a spinor Bose-Einstein condensate. *Phys Rev A* 77:023616.

21. Hamley C, Gerving C, Hoang T, Bookjans E, Chapman M (2012) Spin-nematic squeezed vacuum in a quantum gas. *Nat Phys* 8(4):305–308.

22. Pu H, Law C, Raghavan S, Eberly J, Bigelow N (1999) Spin-mixing dynamics of a spinor Bose-Einstein condensate. *Phys Rev A* 60(2):1463.

23. Chang MS, Qin Q, Zhang W, You L, Chapman MS (2005) Coherent spinor dynamics in a spin-1 Bose condensate. *Nat Phys* 1(2):111–116.

24. Zhang W, Zhou D, Chang MS, Chapman M, You L (2005) Coherent spin mixing dynamics in a spin-1 atomic condensate. *Phys Rev A* 72(1):013602.

25. Lipkin H, Meshkov N, Glick A (1965) Validity of many-body approximation methods for a solvable model: (i). Exact solutions and perturbation theory. *Nucl Phys* 62(2):188–198.

26. Dziarmaga J (2010) Dynamics of a quantum phase transition and relaxation to a steady state. *Adv Phys* 59(6):1063–1189.

27. Levy S, Lahoud E, Shomroni I, Steinhauer J (2007) The a.c. and d.c. Josephson effects in a Bose-Einstein condensate. *Nature* 449(7162):579–583.

28. Trippenbach M, et al. (2008) Spontaneous symmetry breaking of gap solitons and phase transitions in double-well traps. *Phys Rev A* 78:013603.

29. Riedel MF, et al. (2010) Atom-chip-based generation of entanglement for quantum metrology. *Nature* 464(7292):1170–1173.

30. Gross C, Zibold T, Nicklas E, Estève J, Oberthaler MK (2010) Nonlinear atom interferometer surpasses classical precision limit. *Nature* 464(7292):1165–1169.

31. Morrison S, Parkins AS (2008) Collective spin systems in dispersive optical cavity QED: Quantum phase transitions and entanglement. *Phys Rev A* 77:043810.

32. Hoang TM, et al. (2016) Parametric excitation and squeezing in a many-body spinor condensate. *Nat Commun* 7:11233.

33. Black AT, Gomez E, Turner LD, Jung S, Lett PD (2007) Spinor dynamics in an antiferromagnetic spin-1 condensate. *Phys Rev Lett* 99(7):070403.

34. Endres M, et al. (2012) The 'Higgs' amplitude mode at the two-dimensional superfluid/Mott insulator transition. *Nature* 487(7408):454–458.

35. Rüegg Ch, et al. (2008) Quantum magnets under pressure: Controlling elementary excitations in TlCuCl$_3$. *Phys Rev Lett* 100(20):205701.

36. Sooryakumar R, Klein M (1980) Raman scattering by superconducting-gap excitations and their coupling to charge-density waves. *Phys Rev Lett* 45(8):660.

37. Matsunaga R, et al. (2014) Light-induced collective pseudospin precession resonating with Higgs mode in a superconductor. *Science* 345(6201):1145–1149.

38. Sherman D, et al. (2015) The Higgs mode in disordered superconductors close to a quantum phase transition. *Nat Phys* 11:188–192.

39. Pekker D, Varma C (2015) Amplitude/Higgs modes in condensed matter physics. *Annu Rev Condens Matter Phys* 6(1):269–297.

40. Jiang J, Zhao L, Webb M, Liu Y (2014) Mapping the phase diagram of spinor condensates via adiabatic quantum phase transitions. *Phys Rev A* 90:023610.

41. Zurek WH, Dorner U, Zoller P (2005) Dynamics of a quantum phase transition. *Phys Rev Lett* 95(10):105701.

42. Damski B, Zurek WH (2008) How to fix a broken symmetry: Quantum dynamics of symmetry restoration in a ferromagnetic Bose-Einstein condensate. *New J Phys* 10(4):045023.

43. Caneva T, Fazio R, Santoro GE (2008) Adiabatic quantum dynamics of the Lipkin-Meshkov-Glick model. *Phys Rev B* 78(10):104426.

44. Altland A, Gurarie V, Kriecherbauer T, Polkovnikov A (2009) Nonadiabaticity and large fluctuations in a many-particle Landau-Zener problem. *Phys Rev A* 79(4):042703.

45. Gerving CS, et al. (2012) Non-equilibrium dynamics of an unstable quantum pendulum explored in a spin-1 Bose-Einstein condensate. *Nat Commun* 3:1169.

46. Hoang TM, et al. (2013) Dynamic stabilization of a quantum many-body spin system. *Phys Rev Lett* 111(9):090403.

47. Landau LD, Lifshitz EM (1976) *Mechanics* (Butterworth-Heinemann, Oxford).

48. Milburn G, Corney J, Wright E, Walls D (1997) Quantum dynamics of an atomic Bose-Einstein condensate in a double-well potential. *Phys Rev A* 55(6):4318.

49. Tonel AP, Links J, Foerster A (2005) Behaviour of the energy gap in a model of Josephson coupled Bose–Einstein condensates. *J Phys Math Gen* 38(31):6879.

50. Solinas P, Ribeiro P, Mosseri R (2008) Dynamical properties across a quantum phase transition in the Lipkin-Meshkov-Glick model. *Phys Rev A* 78(5):052329.

PHYSICS